Mon. Not. R. Astron. Soc. **443**, 2384 – 2390 (2014) Printed 4 August 2014 (MN LATEX style file v2.2)

The redshift distribution of submillimetre galaxies at different wavelengths

J. A. Zavala⋆, I. Aretxaga and D. H. Hughes
Instituto Nacional de Astrofísica, Óptica y Electrónica (INAOE), Luis Enrique Erro 1, Sta. Ma. Tonantzintla, Puebla, Mexico

arXiv:1407.0721v2 [astro-ph.GA] 31 Jul 2014

Accepted 2014 June 26. Received 2014 June 25; in original form 2014 April 1

ABSTRACT

Using simulations we demonstrate that some of the published redshift distributions of submillimetre galaxies (SMGs) at different wavelengths, which were previously reported to be statistically different, are consistent with a parent distribution of the same population of galaxies. The redshift distributions which peak at $z_{med} = 2.9$, 2.6, 2.2, 2.2, and 2.0 for galaxies selected at 2 and 1.1 mm, and 870, 850, and 450 μm respectively, can be derived from a single parent redshift distribution, in contrast with previous studies. The differences can be explained through wavelength selection, depth of the surveys, and to a lesser degree, angular resolution. The main differences are attributed to the temperature of the spectral energy distributions, as shorter-wavelength maps select a hotter population of galaxies. Using the same parent distribution and taking into account lensing bias we can also reproduce the redshift distribution of 1.4 mm-selected ultra-bright galaxies, which peaks at $z_{med} = 3.4$. However, the redshift distribution of 450 μm-selected galaxies in the deepest surveys, which peaks at $z_{med} = 1.4$, cannot be reproduced from the same parent population with just these selection effects. In order to explain this distribution we have to add another population of galaxies, or include different selection biases.

Key words: galaxies: distances and redshifts – galaxies: high redshift – submillimetre: galaxies.

1 INTRODUCTION

The discovery of a large population of bright sources at high redshift through the opening of the submillimetre (submm) and millimetre (mm) wavelength windows (e.g. Smail et al. 1997; Hughes et al. 1998) continues to have a profound impact on our understanding of galaxy evolution in the early Universe. These submm/mm-selected galaxies (hereafter SMGs) are characterized by large far-infrared (FIR) luminosities ($\gtrsim 10^{12}$ L$_\odot$), tremendous star formation rates (SFRs, $\gtrsim 300$ M$_\odot$ yr^{-1}), large gas reservoirs ($\gtrsim 10^{10}$ M$_\odot$), and a number density that is high compared to local ultraluminous infrared galaxies (see reviews by Blain et al. 2002 and Casey et al. 2014).

Due to the steep rise with frequency of the spectral energy distribution (SED) of this population of galaxies on the Rayleigh–Jeans tail ($S_\nu \propto \nu^{3-4}$), the FIR peak is redshifted into the sub-mm/mm observing bands with increasing distance, resulting in a strong negative k-correction that roughly cancels the effects of cosmological dimming with redshift for observations at $\lambda \geqslant 500\mu$m and within $1 \lesssim z \lesssim 10$ (Blain & Longair 1993). This effect represents a unique opportunity for an unbiased view of star formation over a wide redshift range back to the earlier epochs of structure formation. However, identifying and understanding the nature of these discrete sources has proven to be challenging because of the low angular resolution of single-dish telescopes ($\sim 14 - 35$ arcsec), the faintness of counterparts in the rest-frame optical and ultraviolet bands, and the limited statistics of poor samples (Blain et al. 2002, and references therein). Significant effort, using multi-wavelength observations to identify counterparts, has been made to calculate the redshift distribution of SMGs. The use of high resolution radio continuum and *Spitzer*/Multiband Imaging Photometer for *Spitzer* (MIPS) 24 μm images suffers from a well-known systematic bias against high redshift ($z \gtrsim 3$) sources. Indeed, a large fraction of the counterparts identified using direct interferometric imaging in the mm/submm wavelengths are shown to be extremely faint in nearly all other wavelength bands ($r > 26$, $K > 24$) with little or no radio or *Spitzer*/MIPS 24 μm emission (Iono et al. 2006; Wang et al. 2007; Younger et al. 2007; 2009), and a fraction of high redshift SMGs may have been missed or mis–identified with a foreground source in earlier studies.

Given the ambiguity of identifications through probability considerations, the optical faintness of the counterparts,

⋆ E-mail: zavala@inaoep.mx

and the absence of optical lines in particular redshift ranges, it has been very difficult to estimate the redshift distribution accurately. Where spectroscopic redshifts cannot be measured for large samples of SMGs, deep panchromatic surveys can provide photometric redshifts, however it has not been obvious whether common photometric redshift templates could be applied indiscriminately to all SMG counterparts. Furthermore, it has been shown using submm interferometry with the Atacama Large Millimeter/submillimetre Array (ALMA)[1] that the radio/mid-infrared identification process misses $\sim 45\%$ of SMGs, and of those it claims to find, approximately one-third are incorrect (Hodge et al. 2013). Additionally, some of the published redshift distributions derived from different surveys with different instruments appear to be slightly inconsistent with each other (see Section 2), which adds more uncertainty to the redshift distribution of this population of galaxies.

In this paper, we study the impact that selection effects have on redshift distributions. In Section 2, we summarize the differences among some of the published redshift distributions of the SMG population. In Section 3, we describe the simulations that we have conducted in order to estimate the selection effects (wavelength, depth, and angular resolution of each survey). In Section 4, we present our results derived from the simulations and finally in Section 5, we summarize and discuss our results.

All calculations assume a Λ cold dark matter cosmology with $\Omega_\Lambda = 0.68$, $\Omega_m = 0.32$, and $H_0 = 67.3 \mathrm{kms}^{-1}\mathrm{Mpc}^{-1}$ (Planck Collaboration et al. 2013).

2 PUBLISHED REDSHIFT DISTRIBUTIONS

The redshift distribution of SMGs (and thus their cosmic evolution) is not yet completely understood. A comparison of the redshift distributions from different surveys illustrates this point.

• Chapman et al. (2005) obtained optical spectroscopic redshifts using the Keck I telescope for a sample of 73 SMGs, with a median 850 μm flux density of 5.7 mJy, for which precise positions were obtained through deep Very Large Array radio observations. The galaxies lie at redshifts out to $z = 3.6$, with a median redshift of $z_{med} = 2.2 \pm 0.1$. Furthermore, modelling a purely submm flux-limited sample, based on the expected selection function for their radio-identified sample, they derived a median redshift of 2.3. The parent sample of SMGs used for this survey consists of 150 sources detected at 850 μm (S/N > 3.0) with the Submillimetre Common-User Bolometer Array (SCUBA) on the James Clerk Maxwell Telescope (JCMT, $\theta \approx 14.5$ arcsec) in seven separate fields with a median depth of $\sigma_{850} \sim 1.9$ mJy/beam (according to the median flux density limit of the subset).

• Wardlow et al. (2011) derived photometric redshifts from 17 optical to mid-infrared photometric bands for 78 robust radio, 24 μm and *Spitzer*/Infrared Array Camera (IRAC) counterparts to 72 of the 126 SMGs selected at 870 μm (S/N > 3.7) by the Large APEX Bolometer Camera (LABOCA) Extended *Chandra Deep Field*–South Submillimetre Survey (Weiß et al. 2009) on the Atacama Pathfinder EXperiment (APEX) 12-m telescope ($\theta \approx 19$ arcsec, $\sigma_{870} \sim 1.2$ mJy/beam). The median photometric redshift of the identified SMGs is $z_{med} = 2.2 \pm 0.1$ with $\sim 15\%$ high-redshift ($z \geqslant 3$) SMGs. However, a statistical analysis of sources in the error circles of unidentified SMGs reveals a population of possible counterparts, which added to the identified SMGs shifts the median redshift to $z_{med} = 2.5 \pm 0.2$.

• Yun et al. (2012) reported a redshift distribution with median redshift of $z_{med} \approx 2.6$ with a significant high-redshift tail of $\sim 20\%$ at $z \geqslant 3.3$ for 78 SMGs detected with AzTEC at 1.1 mm (S/N > 3.5) in the Great Observatories Origins Deep Survey-South (GOODS-S) on the Atacama Submillimetre Telescope Experiment (ASTE), ($\theta \approx 30$ arcsec, $\sigma_{1.1} \sim 0.6$ mJy/beam; Scott et al. 2010), and the Great Observatories Origins Deep Survey-North (GOODS-N) on JCMT ($\theta \approx 18$ arcsec, $\sigma_{1.1} \sim 1.0$ mJy/beam, Perera et al. 2008). The photometric redshifts were derived by analysing the SEDs obtained from deep radio continuum, *Spitzer*/MIPS and IRAC, and LABOCA 870 μm data, and complementing the sample with a subset of sources with available spectroscopic redshifts.

• Using ALMA observations, Weiß et al. (2013) found a median redshift of $z_{med} = 3.4$ (taking all ambiguous sources to be at their lowest redshift option) for a survey of 26 strongly lensed dusty star-forming galaxies selected with the South Pole Telescope ($\theta \approx 1$ arcmin, $\sigma_{1.4} \sim 4$ mJy/beam) at 1.4 mm. The sources were selected to have $\mathrm{S}_{1.4mm} > 20$ mJy and a dust-like spectrum and, in order to remove low-z sources, not have bright radio ($\mathrm{S}_{843MHz} < 6$ mJy) or FIR counterparts ($\mathrm{S}_{100\mu m} < 1$ Jy, $\mathrm{S}_{60\mu m} < 200$ mJy). They found one or more spectral features in 23 sources yielding an $\sim 90\%$ detection rate for this survey with a secure redshift for $\sim 70\%$ of the sample. Studying the magnification factors, the sample is expected to cover intrinsic flux densities of $\mathrm{S}_{1.4mm} = 1.0 - 3.0$ mJy.

• Roseboom et al. (2013) present the photometric redshift of 450–μm–selected sources (S/N > 4.0), showing a broad peak in the redshift range $1 < z < 3$, and a median of $z_{med} = 1.4$, combining SCUBA-2 photometry, *Herschel*/Spectral and Photometric Imaging Receiver data from the *Herschel* Multi-tiered Extragalactic Survey , *Spitzer*, and *Hubble Space Telescope* Wide Field Camera 3 photometry. The sample consists of sources detected in the SCUBA-2 Cosmology Legacy Survey (S2CLS)[2] conducted with the JCMT ($\theta \approx 7.5$ arcsec) combining observations on the Ultra Deep Survey (UDS) and the Cosmological Evolution Survey (COSMOS; Geach et al. 2013) fields to a typical central depth of $\sigma \approx 1.5$ mJy/beam (although the noise is increasing in the radial direction).

• Casey et al. (2013) derived optical/near-infrared redshift distributions in the COSMOS field that peak at $z_{med} = 1.95 \pm 0.19$ for 450 μm-selected galaxies and $z_{med} = 2.16 \pm 0.11$ for 850 μm-selected galaxies (S/N > 3.6). The two samples occupy similar areas of the parameter space in redshift and luminosity, while their median SED peak-wavelengths differ by an amount consistent with a difference in dust temperature $\Delta T_{dust} = 8 - 12$ K. The galaxies were ex-

[1] www.almaobservatory.org

[2] http://www.jach.hawaii.edu/JCMT/surveys/Cosmology.html

tracted from deep ($\sigma_{450} \approx 4.13$ mJy/beam and $\sigma_{850} \approx 0.80$ mJy/beam) observations with SCUBA-2/JCMT ($\theta \approx 7.5$ and $\theta \approx 14.5$ arcsec for 450 and 850 μm, respectively).

• Finally, Staguhn et al. (2013) presented the first deep ($\sigma_{2.0} \approx 0.14$ mJy/beam in the central region) map at 2 mm wavelength centred on the *Hubble Deep Field* using the Goddard-IRAM Superconducting 2 Millimeter Observer (GISMO) at the IRAM telescope ($\theta \approx 17.5$ arcsec). The median redshift of the seven sources (S/N > 3.0) with counterparts of known redshifts is $z_{med} = 2.91 \pm 0.94$.

As we can see, the redshift distributions derived from different surveys achieved with different telescopes show significant differences. Yun et al. (2012) conducted a Kolmogorov-Smirnov test between their redshift distribution, Chapman et al. (2005) distribution, and the 850–μm–selected Aretxaga et al. (2007) distribution, finding that the Chapman et al. distribution is substantially different from the Yun et al. and Aretxaga et al. distributions. In the same way, Chapin et al. (2009) claim that their median redshift of 28 1.1 –mm–selected galaxies of $z_{med} = 2.7$ is statistically distinct from the $z_{med} = 2.2$ measured in Chapman et al. sample. Therefore, it is important to study the impact that selection effects might have on these measured redshift distributions, in order to analyse the origin of the differences found.

3 SIMULATIONS

In this section we simulate maps with properties similar to those from which the published redshift distributions have been derived in order to understand the selection effects (i.e. wavelength of observations, angular resolution and depth of the maps). We use an a priori redshift distribution and compare the a posteriori redshift distribution recovered from each simulated map.

We adopt the source counts at 1.1 mm from Scott et al. (2012) derived from 1.6 deg^2 blank-field surveys with AzTEC, and the redshift distribution measured by Yun et al. (2012) for 78 SMGs detected with AzTEC at 1.1 mm in the GOODS fields (see Section 2). We decide to use these priors because 1.1 mm is the central wavelength of surveys considered (450μm−2mm), and hence it has a better overlap with the population of galaxies detected at other wavelengths. Although there are galaxies detected at other wavelengths that are not detected at 1.1 mm, the conclusion of this paper that the 1.1 mm distribution gives a good approximation to the median of a common parent distribution does not change, for the range considered in this paper (450μm−2mm).

Once we generate maps at 1.1 mm, we can calculate the maps at different wavelengths using a modified blackbody and the redshift for each source. The detectable flux density at an observed frequency ν from a galaxy with luminosity L_ν at redshift z is

$$S_\nu = \frac{1+z}{4\pi D_L^2} \frac{L_{\nu(1+z)}}{L_\nu}, \quad (1)$$

where D_L^2 is the luminosity distance. We adopt a modified blackbody, as the SED of each simulated galaxy, with a temperature distribution that follows the temperature–luminosity relationship parametrized by Casey et al. (2012) (see also Chapman et al. 2005 and Chapin et al. 2009), and alternatively, a random temperature drawn from a Gaussian distribution with $\langle T \rangle = 42 \pm 11$ K, as those measured in deep submm surveys (Roseboom et al. 2013). For the spectral index we use a Gaussian distribution with $\langle \beta \rangle = 1.6 \pm 0.5$ (Roseboom et al. 2013).

We co-add this signal map with a noise map where the noise is represented by a Gaussian with a mean of zero mJy/beam and a standard deviation equal to the 1σ depth of each survey described in Section 2. In the case of the sample of Yun et al. (2012), where the galaxies have been selected from two different surveys, we have adopted the mean depth of both surveys. On the other hand, in the case of Weiß et al. (2013), where the sample consists of lensed galaxies, we have adopted a noise ($1\sigma = 0.6$ mJy) such that the galaxies detected (S/N> 3.5) in our simulated map have a flux density similar to the mean delensed (intrinsic) flux density estimated by Weiß et al. (2013). Finally, in the case of Roseboom et al. (2013), we have simulated a noise map in which the noise increases radially from $\sigma \approx 1.5$ mJy/beam to $\sigma \approx 5$ mJy/beam on the edges, similar to the noise properties in the daisy maps of S2CLS. The remaining surveys are quite uniform and do not need a special treatment of their noise properties.

Finally, we convolve this co-added map with a Gaussian point spread function (PSF) with a full width at half–maximum (FWHM) equal to the angular resolution of the different surveys we want to simulate. In Fig. 1, we show an example of a small field within our simulated maps at different wavelengths, different depths, and different angular resolutions generated with this procedure, and the galaxies detected at S/N> 3.5 in each map. In this example, we show maps at 450 μm, 850 μm, 1.1 mm, and 2 mm with angular resolution and depth similar to the surveys published by Casey et al. (2013), Chapman et al. (2005), Perera et al. (2008), and Staguhn et al. (2013), respectively (see Section 2).

In each realization, we simulate seven maps of 400 sq. arcmin that reproduce the wavelength, depth, and angular resolution of the surveys that we wish to analyse. The size of the maps allows us enough statistics in each realization. Once we have all the simulated maps, the next step is to extract the sources and to calculate the redshift distribution of each map. A source is considered to be recovered in each map if it is detected with S/N > ξ_{tresh} within a search radius equal to the FWHM of the beam, where ξ_{tresh} is the value used in each of the surveys described in Section 2 ($\xi_{tresh} = 3 - 4$). We conduct 100 realizations to estimate the redshift distribution extracted for each map, the median value, and the error on the median calculated as the standard deviation of the median values in each realization.

4 RESULTS

4.1 The redshift distribution

Although we have only one a priori redshift distribution, the extracted redshift distributions from the simulated maps have different shapes (see Fig. 2). The median redshift varies increasingly from $z_{med} = 2.06 \pm 0.10$ to 2.91 ± 0.12 as the wavelength of the simulated maps changes from 450 μm to

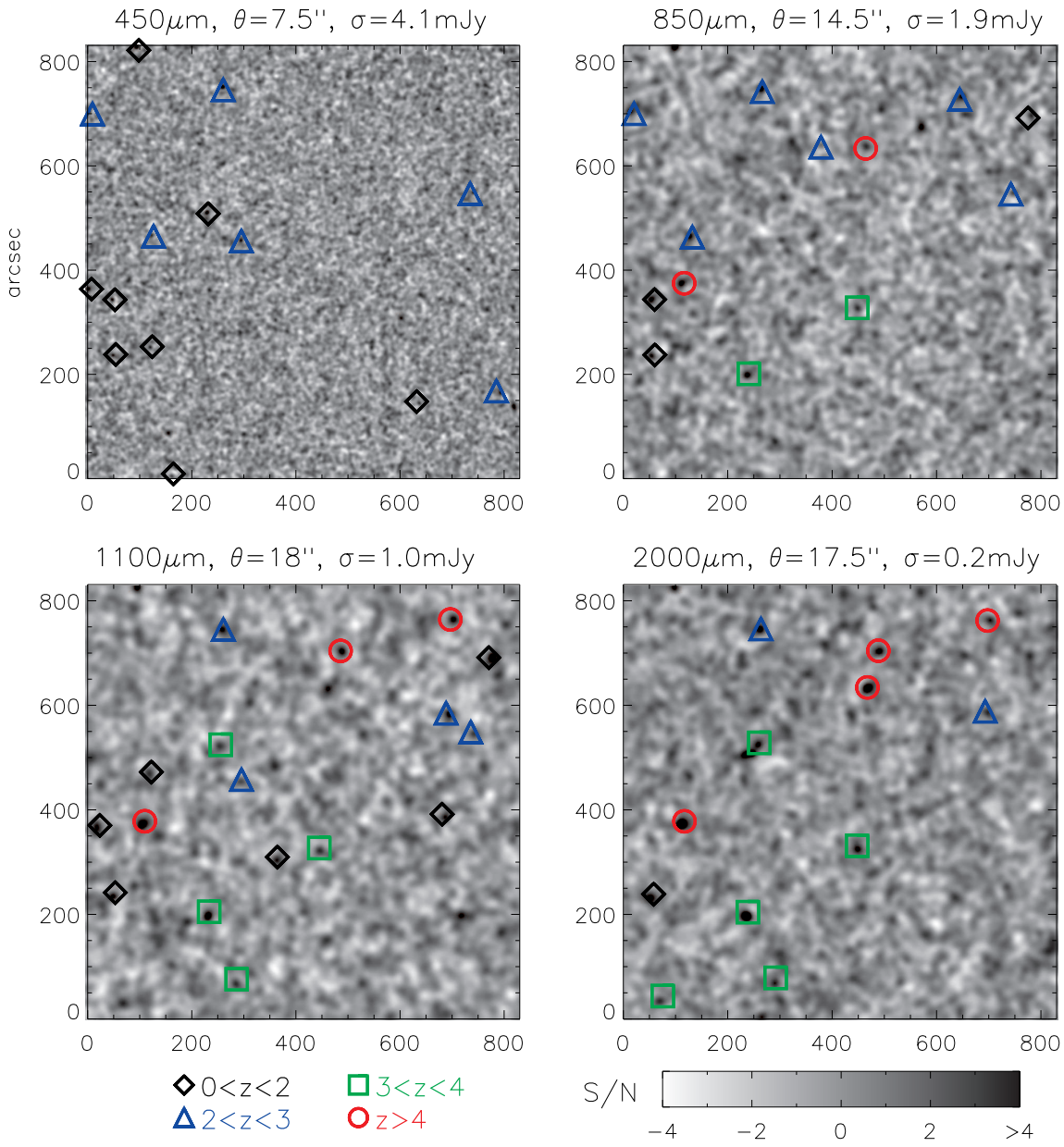

Figure 1. An example of the simulated maps (small region of 800 arsec × 800 arcsec) at different wavelengths, depths and angular resolutions, mocking observations at 450 and 850 μm with SCUBA-2/JCMT, 1.1 mm with AzTEC/JCMT, and 2 mm with GISMO/IRAM. The detected sources (S/N> 3.5) are represented by different symbols, where each symbol (and colour, for the online version) represents the redshift range of the detected galaxy –diamond (black) for $0 < z \leqslant 2$; triangle (blue) for $2 < z \leqslant 3$; square (green) for $3 < z \leqslant 4$; and circle (red) for $z > 4$. The characteristics of each map, wavelength, angular resolution (FWHM), and depth, are displayed at the top of each panel.

2 mm respectively. This result does not depend on whether we assume that the temperature of SMGs follows the same Gaussian distribution for all sources or the temperature-luminosity relationship. We will call this set of redshift distributions, hereafter, the *expected* redshift distributions, since these are the distributions we expect to measure after taking into account selection effects. We will compare these expected redshift distributions with the published distributions.

Casey et al. (2013) derived a redshift distribution with a median of $z_{med} = 1.95 \pm 0.19$ for their 450 μm–map ($\sigma \sim$ 4.1 mJy); in our simulations, we estimate for this survey a redshift distribution with $z_{med} = 2.06 \pm 0.10$, consistent with the published value. This means that we are missing some high-redshift galaxies from the original parent distribution ($z_{med} \approx 2.6$; Yun et al. 2012) through selection effects and for this reason the median is shifted towards lower redshifts.

Chapman et al. (2005) estimated a redshift distribution with $z_{med} = 2.2 \pm 0.2$, whilst we have derived from the sim-

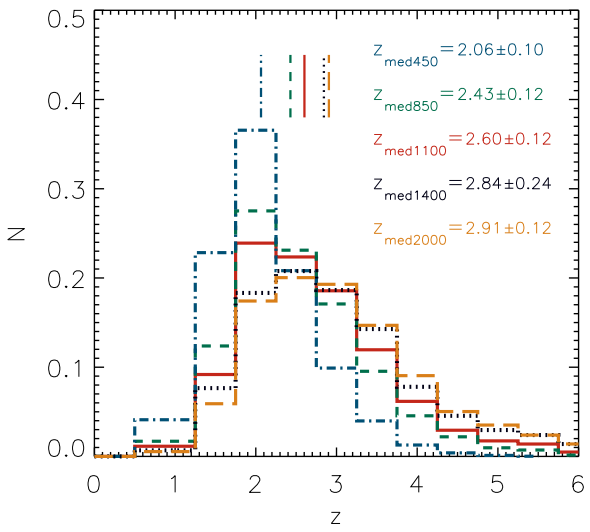

Figure 2. Extracted redshift distributions from the simulated 450 μm–shallow map (dash–dotted blue line), 850 μm–map (short-dashed green line), 1.1 mm–map (solid red line), 1.4 mm–map (dotted black line), and 2 mm–map (long-dashed orange line). Top bars represent the corresponding median values of the distributions.

ulated map a distribution with $z_{med} = 2.43 \pm 0.12$ which is compatible within the error bars with the published value. Chapman et al. proposed a corrected model for their distribution that takes into account the expected radio bias, and suggested a revised $z_{med} \sim 2.3$, in better agreement with our extracted distribution. Hence the redshift distribution of Chapman et al. is also consistent with our a priori redshift distribution.

Wardlow et al. (2011) derived $z_{med} = 2.2 \pm 0.1$ from their 870 μm–survey. A statistical analysis of the unidentified sources, however, shifts the distribution to $z_{med} \approx 2.5 \pm 0.3$ in very good agreement with our expected $z_{med} = 2.46 \pm 0.10$. Moreover, a recent study of the same submillimetre source sample with ALMA, which ensures the photometric redshift of the correct counterparts are used (Simpson et al. 2014) finds the same result with a $z_{med} = 2.5 \pm 0.2$ after correcting for incompleteness.

Staguhn et al. (2013) reported a median redshift of $z_{med} = 2.91 \pm 0.94$ at a wavelength of 2 mm, in very good agreement with the value that we have extracted from our simulated map ($z_{med} = 2.91 \pm 0.12$).

The Yun et al. (2012) distribution is obviously in agreement with our expected distribution, since it is the one we have adopted as the a priori distribution. This confirms that our simulations and the source extraction method are working correctly, since we are recovering the same distribution at this wavelength.

The photometric redshift distribution of Smolčić et al (2012), who found a median redshift of $z_{med} = 3.1 \pm 0.3$ for 17 galaxies detected at 1.1 mm in the COSMOS field, is also within the 68% confidence level bars of our value, but there is an offset from the Yun et al. (2012) distribution. The offset could be due in part to cosmic variance, where the COSMOS field is known to have several notable, very distant $z > 4.5$ galaxies (e.g. Capak et al. 2008; Riechers et al. 2010) as discussed by Casey et al. (2014).

However, there are two distributions which at first are not compatible with our expected redshift distribution for these surveys; these are as follows:

a) The Roseboom et al. (2013) redshift distribution, derived from their deep 450 μm–map, has a median of $z_{med} = 1.4$, which is in disagreement with our expected distribution ($z_{med} = 2.13 \pm 0.08$). It is important to remark the differences between the Roseboom et al. (2013) and the Casey et al. (2013) ($z_{med} = 1.95 \pm 0.19$) redshift distributions because they were extracted from surveys at the same wavelength and angular resolution, but, they peak at different redshifts. This offset is likely due to the difference in depths between both surveys as discussed by Casey et al. (2014). The work by Roseboom et al. is a factor of ~ 3 deeper and therefore they were able to detect fainter galaxies at lower redshift. In conclusion, in order to explain the Roseboom et al. distribution we would need to consider another population of galaxies which lie at lower redshifts and probably with different luminosities and SFRs (i.e. Luminous Infrared Galaxies, LIRGs) than longer–wavelength selected SMGs. The properties that this population of galaxies should have in order to reproduce the redshift distribution are beyond the scope of this paper.

b) The Weiß et al. (2013) redshift distribution is also in disagreement with our expected distribution, since our median redshift is $z_{med} = 2.84 \pm 0.24$. However, as Weiß et al. noted, their selection of bright 1.4 mm sources imposes a requirement that they be gravitationally lensed, effectively suppressing sources at $z < 1.5$ due to the low probability of being lensed at these redshifts. Since our a priori redshift distribution has a significant proportion of sources with $z < 1.5$ ($\sim 5\%$, and $\sim 20\%$ with $z < 2$, where the effect is still significant) we do not expect to have compatible distributions. In order to analyse the lensing bias, we have removed the low-redshift sources from our extracted redshift distribution according to the probability of strong lensing as a function of redshift. In order to estimate this probability, we used a mean source magnification of $\mu = 10$ (the sample has magnifications of $\mu = 5 - 21$) and normalized the lensing probability estimated by Weiß et al. (2013) for this magnification, at $z = 4$, where the probability becomes flat. Once we have removed the low-redshift sources due to the strong lensing effect, the extracted redshift distribution has a median redshift of $z_{med} = 3.09 \pm 0.21$, which is in agreement within the error bars with the derived $z_{med} = 3.4 \pm 0.25$. We have estimated the error in the Weiß et al. median redshift using a bootstrapping method, and taking all ambiguous sources to be at their lowest redshift solution. Simpson et al. (2014) also reached the same conclusion when comparing their 850–μm–selected redshift distribution and the lensing–corrected 1.4–mm–selected redshift distribution.

Aditionally, the galaxies observed by Weiß et al. could be intrinsically brighter than the average SMGs and therefore could lie at higher redshifts as suggested by Koprowski et al. (2013).

We have thus shown that the measured distributions are mostly consistent with a parent distribution with $z_{med} \approx 2.6$, very similar to the redshift distribution of Yun et al. (2012) when taking into account wavelength selection, depth, and angular resolution limitations. We should

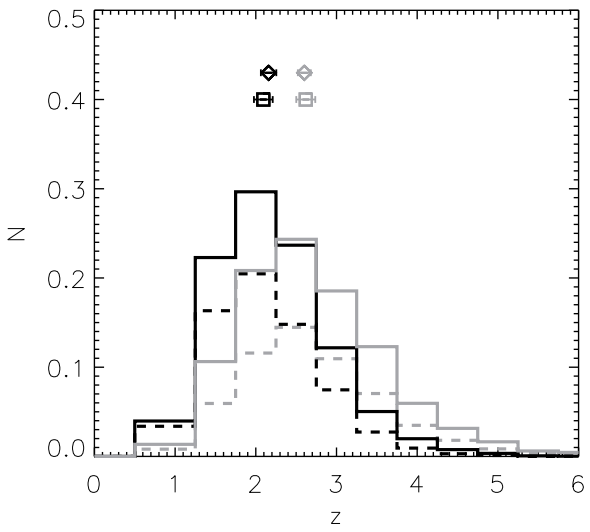

Figure 3. Extracted redshift distributions from the simulated 450 μm-shallow map with a resolution of $\theta = 1''$ (solid black line) and $\theta = 7.5''$ (dashed black line), and from the simulated 1.1 mm-map with a resolution of $\theta = 1''$ (solid gray line) and $\theta = 19''$ (dashed gray line). The median and the error on the median for each distribution (square and diamond for the poorer and better angular resolution maps respectively) are plotted at the top of the graph. The histograms have been scaled by the total number of galaxies extracted from the map with the highest angular resolution, in each wavelength.

stress that we are not considering the difficulties intrinsic to finding multiwavelength counterparts for these sources, or obtaining spectroscopic redshift which could bias the measured redshift distributions observationally. These biases are hence intrinsic to this study and to the adopted prior.

On the other hand, we are also interested in determining which of these parameters is the most crucial factor in imposing differences on the measured redshift distributions. In order to quantify this, we have followed the same procedure as described in Section 3, but now, with an angular resolution of $\theta = 1$ arcsec (comparable to ALMA resolutions) for all the simulated maps.

With this high angular resolution the blending of sources is insignificant and therefore we are able to recover a large fraction of sources in each map. However, the redshift distribution extracted from each simulated map is very similar to the one we measured from the poorer angular resolution maps. In Fig. 3 we show the extracted redshift distribution at 450 μm and 1.1 mm for both, poor ($\theta = 7.5$ and $\theta = 19$ arcsec respectively) and best ($\theta = 1$ arcsec) angular resolutions. At each wavelength, the histograms have been scaled by the total number of galaxies extracted from the map with the highest angular resolution, in order to compare them easily.

The similarity of the histograms confirms that wavelength and depth mainly determine the redshift distribution, and therefore the angular resolution is only a secondary effect in imposing a bias. This result is in agreement with the work of Simpson et al. (2014), who did an ALMA follow-up of the Wardlow et al. (2011) sample finding largely the same redshift distribution with the new high-resolution data. However, the fainter population of galaxies that has not yet been detected with single-dish telescopes (due to the confusion limit) could have a different redshift distribution, and therefore the angular resolution could be an important effect at these smaller flux densities.

4.2 The SED temperature

We have shown that shorter wavelength–maps miss high redshift galaxies. It is also important to understand the differences between the subsets of galaxies selected at different wavelengths. As we have the temperature and emissivity index for each recovered galaxy (grey–body distribution, see Section 3) we can investigate the properties of the SEDs of the galaxies extracted in the different simulated maps. Analysing these properties, we have found that the main difference between the galaxies selected at different wavelengths is the grey–body temperature, where the shorter-wavelength maps select a hotter population. The mean SED peak wavelength monotonically shifts from $109 \pm 4\mu$m to 123 ± 3 (or $T = 46 \pm 2$ to $T = 40 \pm 1$ K) for 450 μm–selected galaxies to 2 mm–selected galaxies, respectively. There is no significant difference between the 1.1 mm, 870 μm, and 850 μm maps, which have a mean SED peak of $118 \pm 4\mu$m (or $T \approx 42 \pm 2$ K).

This effect has been previously discussed by Casey et al. (2013), where they also found that their two samples (SCUBA-2 450 and 850 μm-selected galaxies in the COSMOS field) occupy a similar parameter space in redshift and luminosity, with a difference in the SED peak of $20 - 50\mu$m or a temperature difference of $\Delta T_{dust} = 8 - 12$ K, consistent, within the error bars, with our simulations.

4.3 The K–S test

A common method to compare distributions is the Kolmogorov–Smirnov (K-S) test which tells us the probability that two distributions are drawn from the same parent distribution. We have applied this test to all the pairs of redshift distributions extracted from the different simulated maps. In order to compare with the results from previous studies we have chosen 70 random sources for each simulated map and then we have applied the K-S test to these subsamples. The results are summarized in Table 1.

As can be seen in Table 1, we can reject with better than 99 per cent confidence the hypothesis that the subsample of 450–μm–selected galaxies has a common parent redshift distribution with the subsamples extracted from longer–wavelength simulated maps, even when we know that all these distributions have been generated adopting the same parent distribution. The same hypothesis for other wavelengths cannot be rejected with such a high confidence. Hence, if we want to know that if two distributions extracted from surveys carried out at different wavelengths are compatible with a common parent distribution, one should implement simulations similar to those described here, since the K–S test is not able to take into account the selection effects introduced by the choice of wavelength and depth.

Table 1. K-S test probability that two redshift distributions are drawn from the same parent distribution. A subset of 70 galaxies has been randomly selected from each simulated map.

	450 μm	850 μm	1.1 mm	1.4 mm	2.0 mm
450 μm	–	0.001	3.61e–4	4.43e–7	1.73e–4
850 μm		–	0.857	0.069	0.106
1.1 mm			–	0.326	0.443
1.4 mm				–	0.443

5 DISCUSSION AND CONCLUSIONS

We have analysed the selection effects that wavelength, depth, and angular resolution impose on the extracted redshift distributions from different surveys. We have found that some of the published redshift distributions, which were reported to be inconsistent with each other, are in agreement with a common parent distribution. The differences between these published redshift distributions can be explained by selection effects imprinted mainly by differences in wavelength and depth of the observations.

The median redshifts derived from our simulations ($z_{med} = 2.06 - 2.91$) are in very good agreement with the values previously reported (Chapman et al. 2005; Wardlow et al. 2011; Yun et al. 2012; Casey et al. 2013; Staguhn et al. 2013), which indicate the consistency between the published redshift distributions and our adopted parent distribution, even when some of these distributions have been shown to be statistically inconsistent with each other (Chapin et al. 2009; Yun et al. 2012). We can also reproduce with the same parent distribution the redshift distribution of Weiß et al. (2013) which peaks at $z_{med} = 3.4$, when we take into account the bias imposed by the lensing probability. We conclude that in order to test compatibility of this kind of distributions, which have been extracted from surveys with different selection effects, the best way is to use simulations (similar to the procedure described here).

As expected, and previously described by Casey et al. (2013), the main difference between the galaxies selected at different wavelengths is the SED temperature. The mean SED peak wavelength shifts from $109 \pm 4\mu$m to $123 \pm 3\mu$m (or T= 46 ± 2 to T= 40 ± 1) from 450 μm–selected galaxies to 2 mm–selected galaxies.

Finally, as we have shown here, a comprehensive view and accurate determination of the redshift distribution of SMGs need to be based on the complementarity of multi–wavelength observations from large statistically significant samples. Future multiwavelength large-format cameras, like those designed to operate at the Large Millimeter Telescope, CCAT, and ALMA, will contribute towards this goal as they target similar cosmological fields.

ACKNOWLEDGMENTS

We would like to thank an anonymous referee for a constructive and helpful report, which has significantly improved this paper. This work has been mainly supported by Mexican CONACyT research grants CB-2011-01-167291 and CB-2009-133260. This work was also supported in part by the National Science Foundation under Grant No. PHYS-1066293 and the hospitality of the Aspen Center for Physics. IA would like to thank the participants of the workshop "The Obscured Universe: Dust and Gas in Distant Starburst Galaxies" for discussions and suggestions on this topic.

REFERENCES

Aretxaga, I., Hughes, D. H., Coppin, K., et al., 2007, MNRAS, 379, 1571
Blain, A. W., & Longair, M. S., 1993, MNRAS, 264, 509
Blain, A. W., Smail, I., Ivison, R. J., Kneib, J.-P., & Frayer, D. T., 2002, Phys. Rep., 369, 111
Capak, P., Carilli, C. L., Lee, N., et al., 2008, ApJ, 681, L53
Casey, C. M., Berta, S., Béthermin, M., et al., 2012, ApJ, 761, 140
Casey, C. M., Chen, C.-C., Cowie, L. L., et al., 2013, MNRAS, 436, 1919
Casey, C. M., Narayanan, D., & Cooray, A., 2014, preprint (arXiv:1402.1456)
Chapin, E. L., Pope, A., Scott, D., et al., 2009, MNRAS, 398, 1793
Chapin, E. L., Hughes, D. H., & Aretxaga, I., 2009, MNRAS, 393, 653
Chapman, S. C., Blain, A. W., Smail, I., & Ivison, R. J., 2005, ApJ, 622, 772
Chen, C.-C., Cowie, L. L., Barger, A. J., et al., 2013, ApJ, 762, 81
Dunne, L., Clements, D. L., & Eales, S. A., 2000, MNRAS, 319, 813
Dunne, L., & Eales, S. A., 2001, MNRAS, 327, 697
Geach, J. E., Chapin, E. L., Coppin, K. E. K., et al., 2013, MNRAS, 432, 53
Hodge, J. A., Karim, A., Smail, I., et al., 2013, ApJ, 768, 91
Hughes, D. H., Serjeant, S., Dunlop, J., et al., 1998, Nature, 394, 241
Iono, D., Peck, A. B., Pope, A., et al., 2006, ApJ, 640, L1
Koprowski, M. P., Dunlop, J. S., Michalowski, M. J., et al., 2013, arXiv:1312.1173
Oliver, S. J., Wang, L., Smith, A. J., et al., 2010, A&A, 518, L21
Perera, T. A., Chapin, E. L., Austermann, J. E., et al., 2008, MNRAS, 391, 1227
Planck Collaboration, Ade, P. A. R., Aghanim, N., et al., 2013, arXiv:1303.5076
Riechers, D. A., Capak, P. L., Carilli, C. L., et al., 2010, ApJ, 720, L131
Roseboom, I. G., Dunlop, J. S., Cirasuolo, M., et al., 2013, MNRAS, 436, 430
Scott, K. S., Yun, M. S., Wilson, G. W., et al., 2010, MNRAS, 405, 2260
Scott, K. S., Wilson, G. W., Aretxaga, I., et al., 2012, MNRAS, 423, 575
Simpson, J. M., Swinbank, A. M., Smail, I., et al., 2014, ApJ, 788, 125
Smail, I., Ivison, R. J., & Blain, A. W., 1997, ApJ, 490, L5
Smolčić, V., Aravena, M., Navarrete, F., et al., 2012, A&A, 548, A4
Staguhn, J. G., Kovacs, A., Arendt, R. G., et al., 2013, preprint (arXiv:1311.1485)

Wang, W.-H., Cowie, L. L., van Saders, J., Barger, A. J., & Williams, J. P., 2007, ApJ, 670, L89
Wardlow, J. L., Smail, I., Coppin, K. E. K., et al., 2011, MNRAS, 415, 1479
Weiß, A., Kovács, A., Coppin, K., et al., 2009, ApJ, 707, 1201
Weiß, A., De Breuck, C., Marrone, D. P., et al., 2013, ApJ, 767, 88
Younger, J. D., Fazio, G. G., Huang, J.-S., et al., 2007, ApJ, 671, 1531
Younger, J. D., Fazio, G. G., Huang, J.-S., et al., 2009, ApJ, 704, 803
Yun, M. S., Scott, K. S., Guo, Y., et al., 2012, MNRAS, 420, 957

This paper has been typeset from a TEX/ LATEX file prepared by the author.